Preprint
UCRL-JC-152567

Positron Annihilation Spectroscopy and Small Angle Neutron Scattering Characterization of the Effect of Mn on the Nanostructural Features formed in Irradiated Fe-Cu-Mn Alloys

S.C. Glade, B.D. Wirth, P. Asoka-Kumar, G.R. Odette, P.A. Sterne, R.H. Howell

This article was submitted to
2003 The Metallurgical Society Annual Meeting
San Diego, CA
March 2-6, 2003

February 27, 2003

U.S. Department of Energy
Lawrence Livermore National Laboratory

Positron Annihilation Spectroscopy and Small Angle Neutron Scattering Characterization of the effect of Mn on the Nanostructural Features formed in Irradiated Fe-Cu-Mn Alloys

S.C. Glade[*,1], B.D. Wirth[2], P. Asoka-Kumar[1], G.R. Odette[3], P.A. Sterne[1], and R.H. Howell[1]

[1] Lawrence Livermore National Laboratory, Livermore, CA 94550, USA

[2] University of California, Berkeley, Nuclear Engineering Department, Berkeley, CA 94720, USA

[3] University of California Santa Barbara, Department of Mechanical and Environmental Engineering, Santa Barbara, CA 93106, USA

* corresponding author, glade1@llnl.gov

Abstract

The size, number density and composition of the nanometer defects responsible for the hardening and embrittlement in irradiated Fe-0.9wt.% Cu and Fe-0.9wt.% Cu-1.0wt% Mn model reactor pressure vessel alloys were measured using small angle neutron scattering and positron annihilation spectroscopy. These alloys were irradiated at 290°C to relatively low neutron fluences (E>1 MeV, 6.0×10^{20} to 4.0×10^{21} n/m^2) in order to study the effect of manganese on the nucleation and growth of copper rich precipitates and secondary defect features. Copper rich precipitates were present in both alloys

following irradiation. The Fe-Cu-Mn alloy had smaller precipitates and a larger number density of precipitates, suggesting Mn segregation at the iron matrix-precipitate interface which reduces the interfacial energy and in turn the driving force for coarsening. Mn also retards the precipitation kinetics and inhibits large vacancy cluster formation, suggesting a strong Mn-vacancy interaction which reduces radiation enhanced diffusion.

1. Introduction

The continued operation or lifetime extension of a number of nuclear power plants around the world requires an understanding of the damage imparted to the reactor pressure vessel (RPV) steel by irradiation. This radiation damage causes embrittlement by impeding dislocation motion (Odette 1983, Odette and Lucas 1986). Physically based models and theory combined with characterization methods have yielded information regarding the character of the embrittling features as well as their evolution.

Nanometer sized copper-manganese-nickel rich precipitates have been identified as the primary embrittling feature in RPV steels with greater than 0.05 to 0.1 wt.% Cu (Odette 1983). A secondary embrittling feature has been identified as three-dimensional, sub-nanometer vacancy-solute copper complexes, called stable matrix features. Until recently, the vacancy character of these secondary features had been inferred from simulation results and annealing experiments (Mader 1995, Odette 1983, Odette and Lucas 1986, Wirth *et al.* 1998), but recent positron annihilation spectroscopy experiments have confirmed their vacancy character (Wirth *et al.* 2001 and Wirth *et al.* 2002).

Thermodynamic models predict that manganese will reduce the coherent interfacial energy between the precipitate and the matrix for copper rich precipitates

(CRPs) (Odette and Lucas 1998). This reduction in interfacial energy lowers the barrier to precipitate nucleation and the driving force for precipitate coarsening, resulting in an increase in the number density of precipitates and a decrease in size in Fe-Cu-Mn compared to Fe-Cu alloys. This effect has been experimentally verified with small angle neutron scattering and measurements of yield strength change (Odette and Lucas 1998 and Wirth 1998). However, it is also anticipated that Mn may affect the nucleation rate of copper-rich precipitates due to binding interactions with vacancies, thereby lowering the radiation enhanced diffusion coefficient of copper.

In this article, we present the results of a study of the initial evolution of CRPs in model Fe-Cu-Mn alloys, which form nano-structural features during neutron irradiation similar to those formed in embrittled RPV steels, and the effect of manganese on this evolution. Characterization was preformed using small angle neutron scattering (SANS) and positron annihilation spectroscopy (PAS). This work follows previous measurements on model Fe-Cu and Fe-Cu-Mn alloys irradiated to higher neutron fluences (1×10^{23} n/m^2) (Wirth *et al.* 2001 and Wirth *et al.* 2003).

2. EXPERIMENTAL PROCEDURE

2.1 Materials and Irradiations

The alloys used in this study were binary and ternary model alloys with nominal compositions (in weight percent) of Fe - 0.9% Cu and Fe - 0.9% Cu - 1.0% Mn. The alloys were annealed at 775°C for 17 h followed by a 3 minute salt quench to 450°C prior to air cooling to room temperature to keep the copper in supersaturated solution. Specimens in the form of ~1 cm × ~1cm × ~2mm coupons were irradiated under the

conditions listed in table 1. Note that the highest fluence level, A5, was irradiated with a higher flux (5.0×10^{15} n/m^2-s) than the other irradiation conditions (7.0×10^{14} n/m^2-s).

[Insert table 1 about here]

2.2 Small Angle Neutron Scattering (SANS)

SANS was performed at the 8-meter beamline at the Cold Neutron Research Facility of the National Institute of Standards and Technology (Glinka *et al.* 1986). Samples are measured in a strong magnetic field ($\geq$ 1.8 T $\pm$ 0.1 T) oriented horizontally ($\phi = 0°$) to saturate the α-Fe matrix. This allows for the measurement of both nuclear (N) and magnetic (M) neutron scattering due to scattering length density differences between the α-Fe matrix and the scattering feature. The neutron scattering at small angles ($\theta \leq 8°$) was measured from a well collimated beam of cold neutrons (λ=0.5 nm) with a two-dimensional 64x64 cm position sensitive detector positioned ~2 m from the sample.

Assuming that the features formed under irradiation, namely the nanometer Cu and Cu-Mn precipitates and sub-nanometer secondary features, are spherical and non-magnetic in a saturated ferromagnetic iron matrix, log-normal size distributions of one or two spherical scattering features are fit to the absolute scattering cross section data, which provides the mean size, number density (N_d), and volume fraction (f_v) of the scattering feature(s). Furthermore, estimates of the scattering feature composition can be made from the measured magnetic to nuclear scattering ratio (M/N). More details regarding the SANS experiments and data analysis can be found in (Wirth, *et al.* 2001 , Wirth *et al.* 2003, and Miller *et al.* 2003).

2.3 Positron Annihilation Spectroscopy (PAS)

PAS is a well-established technique for detecting open volume regions of a material (Hautojärvi 1979), as well as the chemical identity of the elements surrounding these open volume regions (Asoka-Kumar *et al.* 1996). A positron is the antiparticle of an electron, with the same mass (511 keV/c^2), but a positive charge. After positron injection into a metal, the positron quickly dissipates its kinetic energy in scattering events and reaches thermal equilibrium (within ~ 3 picoseconds). Due to its positive charge, the positron experiences a repulsive force from ionic cores and an attractive force from electrons, open volume defects, and regions of increased positron affinity. Ultimately, the positron annihilates with an electron, predominantly producing two 511 keV gamma rays traveling in opposite directions.

Additionally, each element has a unique positron affinity and the positron will preferentially localize in regions of high positron affinity. In this study, the positron affinities of the elements in the alloys are: Fe, -3.84 eV; Cu, -4.81 eV; and Mn, -3.72 eV (Puska and Nieminen 1994). As shown by Nagai *et al.* (2000), clusters of copper as small as 5-10 atoms in an iron matrix will localize the positron and effectively act as a positron trap. Two PAS techniques were used in this study. In positron annihilation lifetime spectroscopy (PALS) the interval between implantation of the positron into a material and its annihilation, as detected by the two 511 keV gamma rays, is measured. By decomposing the lifetime spectrum into one to three distinct lifetime components, the positron lifetime in a material is obtained, with the positron lifetime being characteristic of the positron end-state, or trapping site. Multiple lifetimes are present if one or more trapping defects exist. Positron lifetime correlates with vacancy-cluster (open-volume

region) size up to a saturation value characteristic of a planar free surface, as described in more detail by Hautojärvi and Corbel (1995).

The two annihilation gamma rays are not actually at 511 keV, due to the momentum component of the electron-positron pair in the direction of the gamma ray emission; these gamma rays are Doppler shifted, one blue shifted and one red shifted, by an amount of energy $\Delta E = \frac{1}{2} p_L c$, where p_L is the longitudinal component of the electron positron momentum in the direction of the gamma ray emission and c is the speed of light. Measurement of both annihilation gamma rays in coincidence allows for precise determination of the Doppler shift, and thus a measurement of the Orbital Electron Momentum Spectra (OEMS) (Asoka-Kumar *et al.* 1996). Each element has a characteristic orbital electron momentum spectrum, resulting from the combination of core and valence electron momentum. Core electrons are more tightly bound to atoms and have a higher electron momentum than valence electrons, making the high momentum region of the OEMS most useful for elemental specificity. By theoretically calculating the orbital electron momentum spectra (Sterne *et al.* 2002) or measuring the orbital electron momentum spectra of pure elements, a determination of the chemical identity of the elements in the vicinity of the annihilating positron can be obtained.

Two experimental facilities exist at Lawrence Livermore National Laboratory for PALS and OEMS. A high-energy monoenergetic positron beam is formed using positrons emitted from a ^{22}Na source placed at the terminal of a 3 MeV electrostatic accelerator (Howell *et al.* 1999). The positron beam (with a typical intensity of 5×10^5 positrons/s) emerging from the accelerator column is focused by a thin solenoid and exits the vacuum through a 25 μm thick Al window. The positrons enter a specimen either

directly or after passing through a 2 mm thick scintillator, which provides a start signal for positron lifetime measurements. The positron penetration depth is ~2-3mm, and allows bulk property measurements without significant contributions from near-surface regions. The annihilation gamma rays are detected using detectors positioned co-linear (for PALS) or perpendicular (for PALS and OEMS) with respect to the positron beam. The use of a high energy positron beam allows for bulk specimen characterization, which does not need to be in vacuum, and improves the signal to noise ratio by eliminating background radiation from the radioactive positron source.

The second experimental facility is one in which positrons emitted from a ^{22}Na radioactive source are confined and transported to the sample using a strong magnetic field (~1.0 kG). The positrons have a kinetic energy of ~300 keV, giving a maximum penetration depth in materials of ~30 μm. This setup is used for OEMS measurements on bulk specimens, as well as performing magnetic measurements by using the natural spin polarization of radioactively emitted positrons (spin-polarized, magnetic positron annihilation measurements) (Asoka-Kumar *et al.* 2002).

For a material placed in a magnetic field, the magnetic moment is defined by the net difference of electron spins that align parallel (also known as majority electrons) and anti-parallel (minority electrons) to the magnetic field. For the spin-polarized, magnetic positron annihilation measurements, the OEMS is measured before and after a magnetic field polarity reversal. The positron spin is parallel to its momentum (for positrons emitted from a ^{22}Na source, as in this case); by changing the magnetic field polarity, the spins of the majority and minority electrons in the specimen will change direction. Plotting the resulting fraction of annihilations with high momentum (1 - 4 atomic units –

a.u.) versus low momentum (< 0.38 a.u.) electrons for both magnetic field polarities, the two data points (magnetic field parallel and anti-parallel) will super-impose if the region in which the positron annihilates is non-magnetic and diverge if the region is magnetic.

3. EXPERIMENTAL RESULTS AND DISCUSSION

3.1 SANS Results

The results of the SANS data analysis for feature radius, number density and volume fraction are presented in figure 1, including data on the change in yield strength of the irradiated specimens compared with a reference specimen. The measured magnetic to nuclear scattering ratios are presented in table 2. Figure 1a plots the mean radius of precipitates versus increasing dose and shows that the precipitate size increases slightly in the Fe-Cu-Mn alloy, with an average value of approximately 0.76 nm. However, the precipitates in the Fe-Cu alloy are much larger, and exhibit a significant variation in size with fluence, with the mean radius ranging from 1.7 to 2.6 nm.

Figure 1b plots the variation in number density (N_d) with increasing fluence. The number density of the Fe-Cu alloy is relatively constant at about 1×10^{23} m^{-3}, while the number density of the Fe-Cu-Mn alloy is initially lower and then increases from 1×10^{23} m^{-2} to 1×10^{24} m^{-2} .

Figure 1c plots the precipitate volume fraction (f_v) versus fluence. In both alloys, the volume fraction increases until about 2.3×10^{21} n/m^2 and then remains approximately constant or falls slightly. Notably, the precipitate volume fractions are much larger in the Fe-Cu alloy, ranging from 0.38 to 0.72%, than in the Fe-Cu-Mn alloy, with values from 0.03 to 0.24%.

Figure 1d plots the change in the yield strength of the irradiated specimens compared to an un-irradiated reference specimen. The trend in the change in yield strength with increasing fluence follows the trend in the volume fraction, figure 1d. This is expected, as shown by (reference). Also, this change in yield strength shows that the alloys are becoming more brittle with increasing fluence.

[Insert figure 1 about here]

The scattering features in all of the irradiated alloys are consistent with copper rich precipitates. The measured magnetic to nuclear (M/N) scattering ratio, table 2, averages 5.2 for the Fe-Cu alloy and 3.3 for the Fe-Cu-Mn alloy. In the Fe-Cu alloy system, a precipitate containing ~94% Cu and 6% vacant sites corresponds to a M/N of 5.2, as does a precipitate containing 10% Fe, 80.6% Cu and 9.4% vacant sites. The lower values of the M/N ratio in the Fe-Cu-Mn alloy are consistent with Mn addition to the precipitates. In fact, a precipitate with a composition of 89.0% Cu and 11.0% Mn corresponds to a M/N of 3.2. This lower M/N ratio is also consistent with precipitates of composition 10.0% Fe, 77.0% Cu and 13.0% Mn, or 10.0% Fe, 75.4% Cu, 9.6% Mn, and 5.0% vacant sites.

3.2 PAS Results

OEMS for the Fe-Cu and the Fe-Cu-Mn alloys are presented in figure 2. The data in this figure has been divided by the corresponding spectrum from the un-irradiated reference specimen in order to emphasize the high momentum portion of the spectra; i.e., $n(p_L)/n(p_L)_{reference}$. Thus, the un-irradiated reference specimen would have a horizontal

line at 1 if plotted in this figure. Also included in the figure is a spectrum of well-annealed elemental copper normalized to the relevant reference specimen. The spectra for the irradiated alloys clearly show evidence of copper, as seen by the peak at $p_L \sim 3.5$ atomic units (a.u.). OEMS for the Fe-Cu alloy, shown in figure 2a, reveal an increasing peak in the low momentum spectrum ($p_L < 0.75$ a.u.) with increasing neutron fluence, while the broad peak at $p_L \cong 3.5$ a.u. decreases. The increase in the low momentum portion results from an increased fraction of positrons annihilating with valence electrons, and indicates positron localization and annihilation at vacancy clusters. The OEMS evolution with increasing fluence, that is an increase at $p_L < 0.75$ a.u. and a decrease $p_L \cong 3.5$ a.u., is consistent with a two-defect trapping model, where the dominant positron trap evolves between the copper rich precipitates (~3.5 a.u.) and a secondary feature (< ~0.75 a.u.), identified as vacancy solute clusters. This change in the low momentum fraction and its identification as trapping and annihilation at vacancy clusters is confirmed by the magnetic polarization along with positron lifetime measurements, plotted in figures 3 and 4 and discussed below.

The measured OEMS for the Fe-Cu-Mn alloy, shown in figure 2b, does not vary with fluence and is quite similar to the shape of the copper spectrum, although with a slightly decreased magnitude. These spectra are indicative of CRPs that are highly enriched in Cu. Notably, annihilations with either Fe or Mn would reduce the OEMS magnitude, with values < 1.0 for Mn relative to Fe at high electron momentum ($p_L > 2$ a.u.). Thus, an interpretation of CRP composition of ~87.4% Cu, 12.6% Mn obtained from the measured M/N ratio by SANS is consistent with the measured OEMS spectrum. Another interesting note is the lack of a peak in the OEMS spectra at low momentum

values (and a corresponding lack of long lifetime components discussed below) in the Fe-Cu-Mn alloy. This may suggest that the effect of Mn is to retard the formation of large vacancy-solute clusters; or, alternately, the effect of Mn on the CRP population increases the number density to a level where all of the positrons localize in the CRPs.

[Insert figure 2 about here]

The results of the spin-polarized, magnetic positron annihilation measurements are presented in figure 3. For both the Fe-Cu and the Fe-Cu-Mn alloys, the un-irradiated reference specimen has a split in the two points with the magnetic field oriented parallel and anti-parallel to the positron spin, similar to the iron sample. For all the irradiated specimens, the two points nearly super-impose with a reduction in the splitting. This lack of splitting of the two points is an indication of non-magnetic behavior at the region of positron annihilation. Figure 3 also shows that the fraction of annihilations with low momentum electrons increases with increasing fluence for the Fe-Cu alloy, again a characteristic of increasing annihilations with valence electrons and indicative of trapping in vacancy clusters.

Positron annihilations with high momentum electrons (orbital electrons) give a measure of the chemical composition of the region in which the positron annihilates. Positron annihilation with low momentum electrons (valence electrons) give a measure of the vacancy character of the region in which the position annihilates. When OEMS data are plotted as in figure 3, positron annihilations at a single type of defect at varying concentrations will lie along a single line. As shown by the dotted lines in figure 3,

drawn to guide the eye, the un-irradiated control specimens are consistent with a single line with elemental Fe while the irradiated samples are consistent with a different single line with elemental Cu. This simple analysis also strongly indicates the highly enriched nature of Cu in the precipitates.

[Insert figure 3 about here]

Positron lifetime annihilation spectroscopy data is presented in figure 4. For the Fe-Cu alloy, figure 4a, the mean positron lifetime increases with increasing neutron fluence. The positron lifetime fitting procedure yielded two distinct lifetime components at a fluence of 1.0×10^{21} n/m^2, with the second lifetime component of 222 ps consistent with small vacancy clusters. The fitting procedure yielded three lifetime components for the specimens irradiated to higher fluence, with the two longer lifetime components (of approximately 210 and 375 ps) consistent with small and larger vacancy clusters, respectively. The OEMS results of figures 2 and 3 may also provide an indication that the vacancy clusters are complexed with Cu solutes.

The bulk lifetime of 108 ps in the Fe-Cu reference specimen increases to ~111 ps in the irradiated specimens. To understand this change, we have performed positron lifetime calculations using a recently developed electronic structure method (Sterne et al. 1999). We find that the 108 ps reference specimen lifetime is consistent with the calculated lifetime of 107 ps for bulk Fe, and that the ~111 ps value in irradiated samples is consistent with the calculated lifetime of 111 ps for Cu in a BCC structure with the Fe lattice constant. This is consistent with coherent Cu precipitates in Fe. With increasing

irradiation, vacancy solute clusters are growing, as evidenced by the larger intensities for the longer lifetime components in the specimen.

The mean lifetime in all of the Fe-Cu-Mn irradiated alloys, figure 4b, was 116 ps, compared to 109 ps for the reference alloy. The positron lifetime fitting procedure yielded only one lifetime component in all of the Fe-Cu-Mn alloys.

[Insert figure 4 about here]

3.3 Discussion

As indicated by both the SANS and the PAS characterization, CRPs, which are not present in the un-irradiated alloys, rapidly form under irradiation, although the formation of a high volume fraction is delayed by the presence of Mn in the alloy. Vacancy-Cu solute cluster complexes were identified in the Fe-Cu alloy, but not in the Fe-Cu-Mn alloy. The fact that no vacancy-Cu solute cluster complexes are present in the Fe-Cu-Mn alloy, as measured by PAS, indicates that Mn is retarding the formation of large vacancy clusters. The influence of Mn on the CRPs is a relatively clear indication of an interaction between the Mn and individual vacancies, which reduces the overall vacancy diffusion and the corresponding radiation enhanced diffusion of copper necessary for CRP formation in this alloy. However, the mechanism by which Mn slows the kinetics of CRP growth in irradiated steels is not entirely evident at this time.

The effect of Mn on CRP evolution is also evident in smaller, more numerous (i.e., higher number density) precipitates formed in the Fe-Cu-Mn alloy. The larger, less numerous precipitates in the Fe-Cu alloy may indicate an increased rate of coarsening, as

well as an earlier nucleation, without the presence of Mn. Additionally, the smaller size and larger number density of scattering features observed in the Fe-Cu-Mn alloy may be due to Mn reducing the driving force for coarsening by reducing the interfacial energy at the iron matrix – copper precipitate interface.

4. Summary

The use of SANS and PAS to characterize irradiated Fe-Cu and Fe-Cu-Mn reactor pressure vessel model alloys indicates that additional alloying elements can significantly affect the nucleation and growth of copper rich precipitates and vacancy solute clusters. The Mn in the Fe-Cu-Mn alloys retards the kinetics of precipitation at low fluence and inhibits the formation of large vacancy clusters, suggesting a strong Mn-vacancy interaction which reduces the radiation enhanced diffusion. Mn also decreases the precipitate size and increases precipitate number density, suggesting that Mn lowers the interfacial energy at the iron matrix-copper precipitate interface, which in turn reduces the driving force for coarsening.

The remaining positron annihilation spectroscopy measurements and a more complete treatment of the data presented in this article will the subject of a future publication.

Acknowledgments

This work was performed under the auspices of the U. S. Department of Energy by the University of California, Lawrence Livermore National Laboratory under Contract No. W-7405-Eng-48 and partially supported by the US Nuclear Regulatory Commission. We

acknowledge the contributions of Doug Klingensmith (UCSB) and Dr. C.J. Glinka (NIST) as well as the support of the National Institute of Standards and Technology, U.S. Department of Commerce, in providing the neutron research facilities used in this work.

References

Asoka-Kumar, P., Alatalo, M., Ghosh, V.J., Kruseman, A.C., Nielsen, B., and Lynn, K.G., 1996, Phys. Rev. Lett. **77**, 2097.

Asoka-Kumar, P., Wirth, B.D., Sterne, P.A., and Odette, G.D., 2002, Phil. Mag. Lett. **82**, 609.

Glinka , C.J., Rowe, J.M., and laRock, J.G., 1986, J. of Applied Crystallography **19**, 427.

Hautojärvi, P. (Editor), 1979, *Positrons in Solids*, (Heildelberg, Topics in Current Physics, Vol. 12)

Hautojärvi, P. and Corbel, C., 1995, Positron Spectroscopy of Solids, Proceedings of the International School of Physics, Course CXXV, edited by A. Dupasquier and A.P. Mills, Jr. (Bologna, Italy: Italian Physical Society), pp.491 – 532.

Howell, R.H., Sterne, P.A., Hartley, J., Cowan, T.E., 1999, *J. Appl. Surf. Sci.* **149**, 103.

Mader, E.V., 1995, *Kinetics of Irradiation Embrittlement and the Post-Irradiation Annealing of Nuclear Reactor Pressure Vessel Steels*, Ph.D. Dissertation, University of California Santa Barbara.

Miller, M.K., B.D. Wirth, and G.R. Odette, 2003, in press, Mat. Sci. and Eng. A.

Nagai, Y., Hasegawa, M., Tang, A., Hempel, A., Yubuta, K., Shimamura, T., Kawazoe, Y., Kawai, A., and Kano, F., 2000, *Phys. Rev. B* **61**, 6574.

Odette, G.R., 1983, *Scripta Met.* **11**, 1183.

Odette, G.R., 1995, Materials Research. Society Symposium Proceedings, Vol 373 (Warrendale, Pennsylvania: Materials Research Society), p. 137.

Odette, G.R. and Lucas, G.E., 1986, *Proceedings of the Second International Symposium on Environmental Degradation of Materials in Nuclear Power Systems – Water Reactors,* edited by J.T.A. Roberts, J.R. Weeks, and G.J. Theus (LaGrange Park, Illinois: American Nuclear Society), p. 345.

Odette, G.R. and Lucas, G.E., 1998, *Radiation Effects & Defects in Solids* **144**, 189.

Puska, M.J. and Nieminen, R.M., 1994, *Rev. Mod.* Phys. **66**, 841.

Sterne, P.A., Pask, J.E., and Klein, B.M., 1999, Appl. Surf. Sci. **149**, 238.

Sterne, P.A., P. Asoka-Kumar, and R.H. Howell, 2002, Appl. Surf. Sci. **194**, 71.

Wirth, B.D., 1998, *On the Character of Nano-Scale Features in Reactor Pressure Vessel Steels Under Neutron Irradiation*, Ph.D. Dissertation, University of California Santa Barbara.

Wirth, B.D., Asoka-Kumar, P., Howell, R.H., Odette, G.R., and Sterne, P.A., 2001, *Mictostructural Processes in Irradiated Materials-2000*, Materials Research. Society Symposium Proceedings, Vol 650 (Warrendale, Pennsylvania: Materials Research Society), pp R6.5.1 –R6.5.6.

Wirth, B.D., Odette, G.R., Asoka-Kumar, P., Howell, R.H., and Sterne, P.A., 2002, *Proceedings of the 10th International Symposium on Environmental Degradation of Materials in Light Water Reactors,* edited by G.S. Was, (National Association of Corrosion Engineers).

Wirth, B.D., Asoka-Kumar, P., Howell, R.H., Odette, G.R., and Sterne, P.A, 2003, "Positron Annihilation Spectroscopy and Small Angle Neutron Scattering Characterization of Nanostructural Features in Irradiated Fe-Cu-Mn Alloys," submitted to Journal of Nuclear Materials.

Tables

table 1 - Neutron irradiation conditions used in this study. All irradiations were performed at T = 290°C.

Irradiation Designation	**neutron flux [ϕ (n/m^2-s)]**	**neutron fluence [ϕt (n/m^2)]**
A1	7. 0×10^{14}	6.0×10^{20}
A2	7.0×10^{14}	1.0×10^{21}
A3	7.0×10^{14}	2.3×10^{21}
A4	7.0×10^{14}	3.2×10^{21}
A5	5.0×10^{15}	4.0×10^{21}

table 2 – Magnetic to nuclear scattering ratio for the irradiated samples.

	Fe-Cu	**Fe-Cu-Mn**
A1	4.5	4.3
A2	5.2	3.2
A3	5.3	3.4
A4	5.5	3.0
A5	5.5	2.8

Figure Captions

figure 1 - Results of SANS data analysis: a) radius, b) number density, and c) volume fraction of scattering features versus neutron fluence. d) shows the change in the tensile yield stress, $\Delta\sigma_y$, compared to an un-irradiated reference specimen. The open symbols at the highest fluence level are to indicate that a higher flux was used in these irradiations. See table 1 for irradiation conditions.

figure 2 - Orbital electron momentum spectra for the a) Fe-Cu and b) Fe-Cu-Mn alloys irradiated under different conditions (table 1). The spectra have been normalized to the corresponding un-irradiated reference specimen. The correspondingly normalized curves of elemental Cu are shown for comparison.

figure 3 - Results of the spin-polarized, magnetic positron annihilation measurements. Positron annihilation fraction with high momentum (1-4 a.u.) versus low momentum (< 0.38 a.u.) electrons, normalized to the total annihilations, for the magnetic field oriented parallel (up triangle) and anti-parallel (down triangle) to the positron polarization. Elemental Fe and Cu are shown with solid symbols. The dotted lines are drawn to guide the eye.

figure 4 - Results of the PALS for the a) Fe-Cu and b) Fe-Cu-Mn alloy. Lifetime for the reference specimens are indicated on the graphs. For the Fe-Cu alloy, the bottom panel shows lifetime, including mean lifetime, while the upper panel shows the intensity of

each lifetime component. Three lifetimes were present in the Fe-Cu alloy at the higher fluence levels, while the Fe-Cu-Mn alloy only exhibited a single lifetime.

figure 1

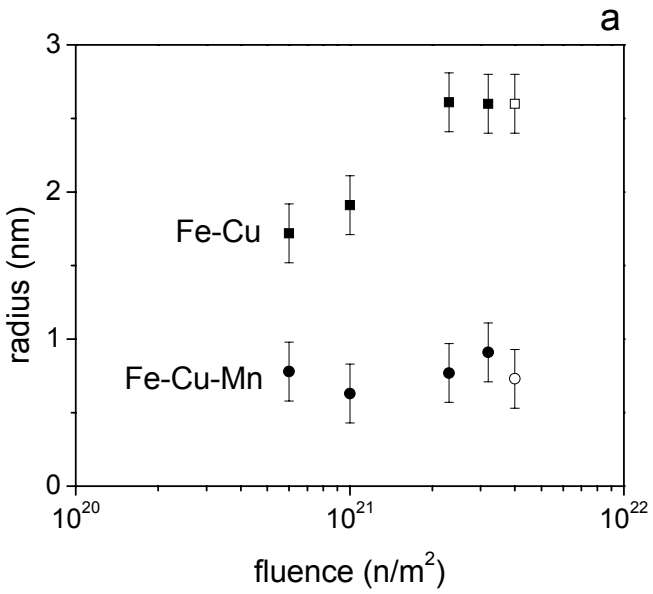
a
3
2
1
0
radius (nm)
Fe-Cu
Fe-Cu-Mn
10^{20}
10^{21}
10^{22}
fluence (n/m^2)

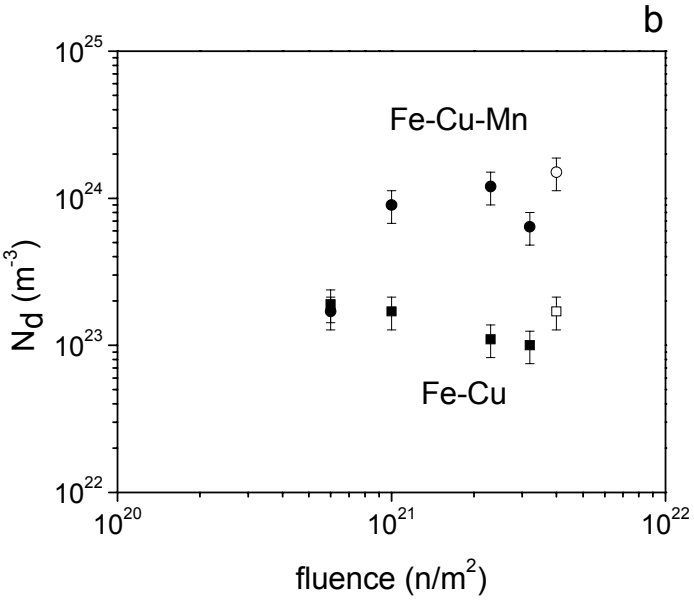
b
10^{25}
10^{24}
10^{23}
10^{22}
N_d (m^{-3})
Fe-Cu-Mn
Fe-Cu
10^{20}
10^{21}
10^{22}
fluence (n/m^2)

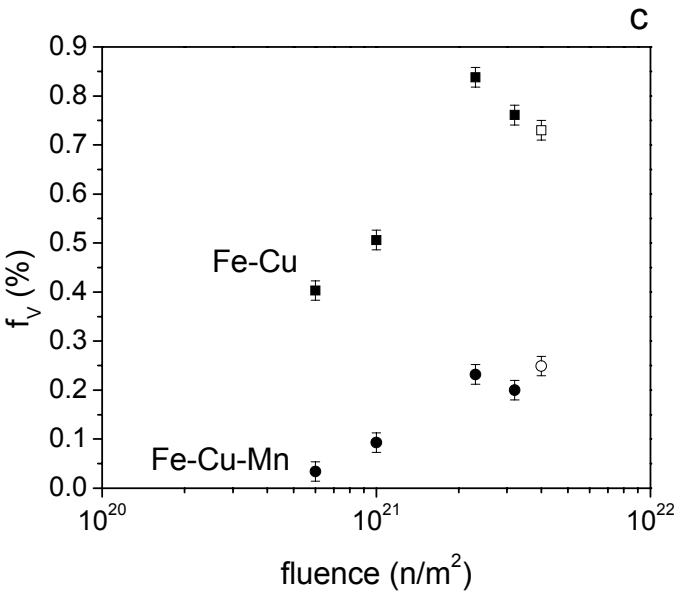
c
0.9
0.8
0.7
0.6
0.5
0.4
0.3
0.2
0.1
0.0
f_V (%)
Fe-Cu
Fe-Cu-Mn
10^{20}
10^{21}
10^{22}
fluence (n/m^2)

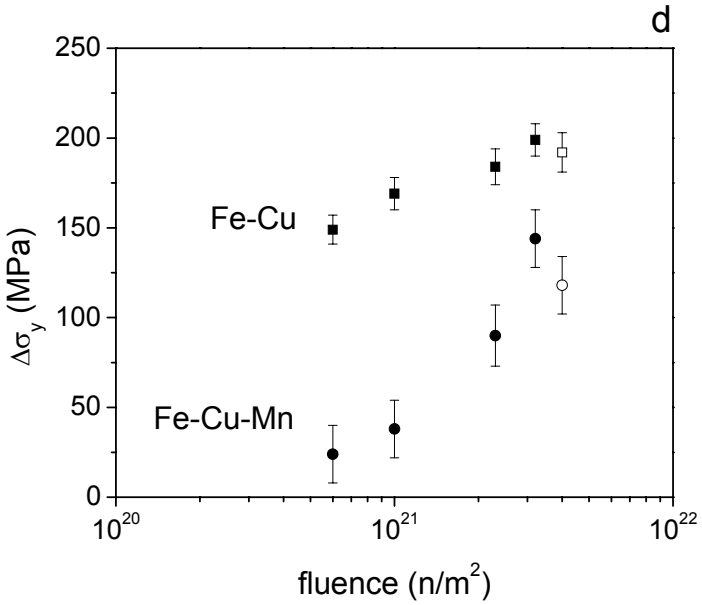
d
250
200
150
100
50
0
$\Delta\sigma_y$ (MPa)
Fe-Cu
Fe-Cu-Mn
10^{20}
10^{21}
10^{22}
fluence (n/m^2)

figure 2

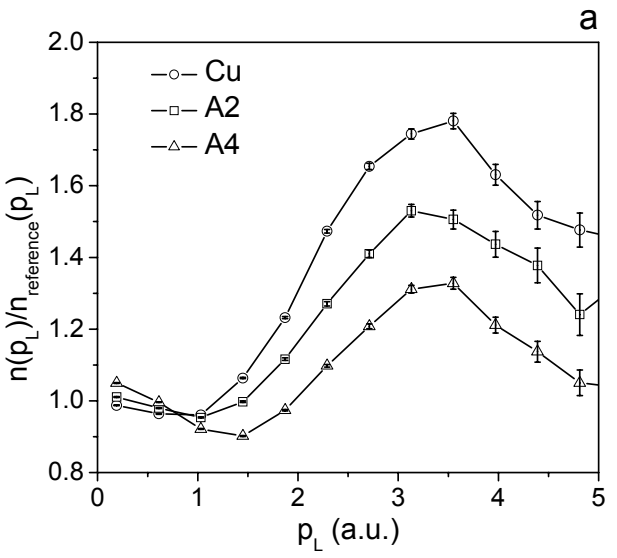
a
Cu
A2
A4
$n(p_L)/n_{reference}(p_L)$
p_L (a.u.)

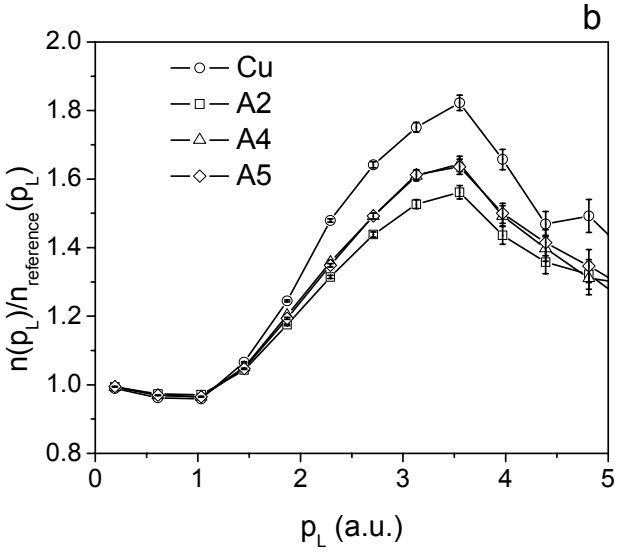
b
Cu
A2
A4
A5
$n(p_L)/n_{reference}(p_L)$
p_L (a.u.)

figure 3

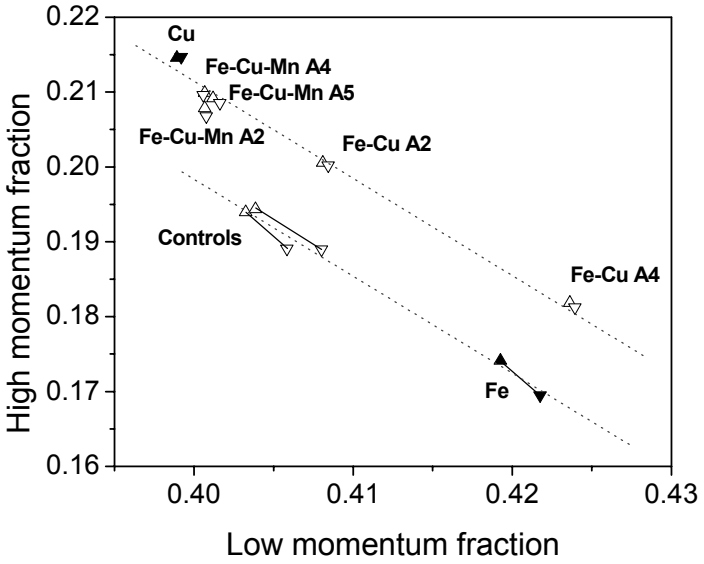
Cu
Fe-Cu-Mn A4
Fe-Cu-Mn A5
Fe-Cu-Mn A2
Fe-Cu A2
Controls
Fe-Cu A4
Fe
High momentum fraction
Low momentum fraction
0.22
0.21
0.20
0.19
0.18
0.17
0.16
0.40
0.41
0.42
0.43

figure 4

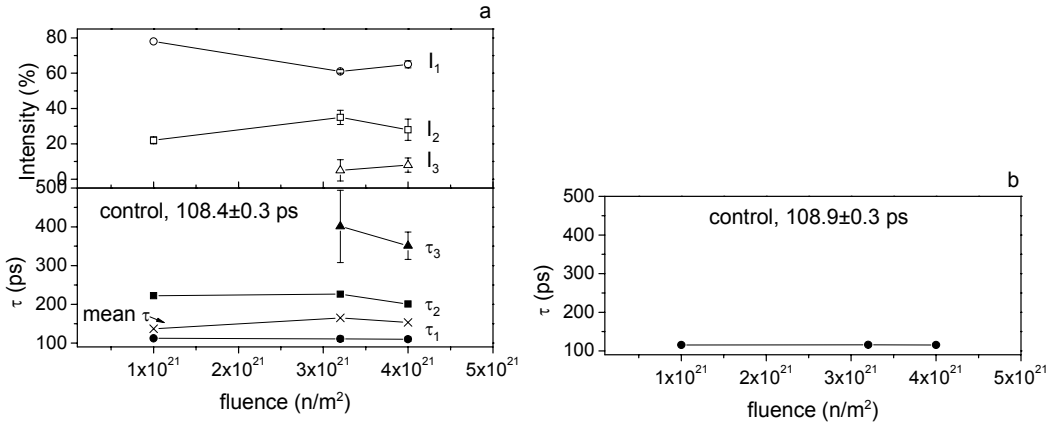
a
Intensity (%)
I1
I2
I3
control, 108.4±0.3 ps
τ (ps)
τ3
τ2
τ1
mean τ
1x10^21
2x10^21
3x10^21
4x10^21
5x10^21
fluence (n/m^2)
b
control, 108.9±0.3 ps
τ (ps)
fluence (n/m^2)